ciently high rate to permit a decrease in rate of a factor of 2 to be detectable.

With the data at hand, it is not obvious which of the sources of deformation are implicated in the slowdown. The deceleration of the deformation sources cannot be spatially uniform because the decrease in deformation rate is spatially variable. However, simultaneous least-squares fitting of the distance measurements to model 2 at approximately bimonthly intervals indicates that no individual component of the model necessarily accounts for the observed deceleration. Nonetheless, the change in deformation rate detected by the two-color geodimeter is clearly discernible (Fig. 2) and must reflect changes in the level of activity at depth (*15*).

REFERENCES AND NOTES

1. J. C. Savage and M. M. Clark, *Science* **217**, 531 (1982); J. C. Savage and M. Lisowski, *J. Geophys. Res.* **89**, 7671 (1984); R. P. Denlinger and F. S. Riley, *ibid.*, p. 8303; R. O. Castle, J. E. Estrem, J. C. Savage, *ibid.*, p. 11507.
2. J. C. Savage and R. S. Cockerham, *J. Geophys. Res.* **89**, 8315 (1984).
3. C. H. Cramer and T. R. Toppozada, *Calif. Div. Mines Geol. Spec. Rep. 150* (1980), p. 91; A. S. Ryall and F. Ryall, *Science* **219**, 1432 (1983); C. O. Sanders, *J. Geophys. Res.* **89**, 8287 (1984).
4. R. A. Bailey, G. B. Dalrymple, M. A. Lanphere, *J. Geophys. Res.* **81**, 125 (1976).
5. A. H. Lachenbruch and J. H. Sass, *Geol. Soc. Am. Mem.* **152**, 209 (1978).
6. C. D. Miller, D. R. Mullineaux, D. R. Crandell, R. A. Bailey, *U.S. Geol. Surv. Circ. 877* (1982); D. P. Hill, R. E. Wallace, R. S. Cockerham, *Earthquake Predict. Res.* **3**, 551 (1985).
7. J. B. Rundle and J. H. Whitcomb, *J. Geophys. Res.* **89**, 9371 (1984).
8. By ranging on two optical wavelengths (red and blue) instead of just one, first-order corrections for variations in the speed of light along the path can be made, yielding distance measurements that are precise to about 0.1 ppm [L. E. Slater and G. R. Huggett, *J. Geophys. Res.* **81**, 6299 (1976)].
9. The instrument used to obtain these data is a new portable version of an observatory-based two-color ranging system that has been used to measure crustal deformation in California near Hollister [G. R. Huggett, L. E. Slater, J. O. Langbein, *J. Geophys. Res.* **82**, 3261 (1977)], Pearblossom (*10*), and most recently Parkfield [L. E. Slater and R. O. Burford, *Eos* **65**, 852 (1984)]. The long-term stability of the portable instrument has been assessed by conducting an extensive series of baseline measurements in parallel with the observatory-based system. For the time interval covered in this report, the only detectable change in the relative instrument scale occurred in the fall of 1983 and has been attributed to component replacements made during October 1983 in the portable instrument [J. O. Langbein, *U.S. Geol. Surv. Open-File Rep. 84-628* (1984), p. 220]. For our analysis, we adjusted the measured distances to account for this observed 0.43 ± 0.06 ppm increase in instrument length scale. Following J. C. Savage and W. H. Prescott [*J. Geophys. Res.* **78**, 6001 (1973)], we assumed the precision of the distance measurements to have the form $\sigma^2 = a^2 + b^2L^2$, where σ is the standard deviation of the error of a single distance measurement, L is the baseline length, and a and b are empirically determined constants. Using the least-squares technique, we fit parabolic functions of time to all the data presented here and determined that a = 0.7 mm and b = 0.12 ppm. This error budget appears to be independent of the averaging interval for periods of 3 to 15 months and is consistent with corresponding results obtained from the intercomparison tests with the observatory-based instrument.
10. J. O. Langbein, M. F. Linker, A. McGarr, L. E. Slater, *Science* **218**, 1217 (1982).
11. J. C. Savage, W. H. Prescott, M. Lisowski, N. E. King, *J. Geophys. Res.* **86**, 6991 (1981).
12. J. E. Estrem, M. Lisowski, J. C. Savage, *J. Geophys. Res.* **90**, 12683 (1986).
13. Although estimates of vertical deformation within the caldera for this interval (*12*) are qualitatively consistent with uplift of the resurgent dome as predicted by either of the models, both models fail the χ^2 test when compared to computed tilt rates alone. However, this inconsistency is neither surprising nor fatal in that vertical geodetic data from volcanic regions are commonly incompatible with simple models constructed to conform with horizontal geodetic data alone [J. H. Dieterich and R. O. Decker, *J. Geophys. Res.* **80**, 4094 (1975)]. With the inclusion of additional model parameters, the degree of model misfit could be improved.
14. G. C. Taylor and W. A. Bryant, *Calif. Div. Mines Geol. Spec. Rep. 150* (1980), p. 49.
15. K. Mogi, *Bull. Earthquake Res. Inst. Tokyo* **36**, 99 (1958).

16. We thank P. Bozek, G. Burton, J. E. Estrem, K. Hudnut, D. Knapp, E. A. Lawrence, P. Levine, M. L. MacKenzie, M. Mann, V. Pease, D. B. Reneau, and A. J. Rigoni for their participation in the field operations; M. D. Clark for support in initiating the field program; L. E. Slater and R. O. Burford for cooperating in the intercomparison tests, which began in early 1980; J. C. Savage for the use of his program for modeling dislocations in an elastic half-space and for early access to the Geodolite data; and D. P. Hill, W. H. Prescott, J. C. Savage, and M. Lisowski for helpful discussions.

24 June 1985; accepted 26 Nover-' 1985

Geometrical Aspects of Sorted Patterned Ground in Recurrently Frozen Soil

KEVIN J. GLEASON, WILLIAM B. KRANTZ, NELSON CAINE, JOHN H. GEORGE, ROBERT D. GUNN

A model for sorted patterned ground shows that some types arise from density-driven Rayleigh free convection that occurs during thawing of water-saturated recurrently frozen soils. The regularly spaced convection cells result in an uneven melting of the underlying ice front. Frost action causes stones to be upthrusted and to form in a pattern on the ground surface that mirrors the corrugation in the underlying ice front. The implications of the water circulation direction in the cells on the sorting process are considered.

"SORTED PATTERNED GROUND" refers to symmetrical forms such as polygons (Fig. 1) or stripes (Fig. 2) that are made prominent because of the segregation of stones and fines resulting from diurnal, seasonal, or other recurrent freeze-thaw cycles in water-saturated soils. These patterns can be found underwater (Fig. 3) as well. A model developed by Ray *et al.* (*1, 2*) explains many features of a broad class of patterned ground. We present new data in support of this model and report further model development describing pattern geometry.

Rayleigh free convection (*3*) is the basis of the model of Ray *et al.* When frozen soil thaws, the potential for free convection exists at least during some portion of the thaw period because of the density inversion for water between 0° and 4°C (*4*). That is, more dense water a few degrees above its freezing point can overlie less dense water at 0°C. A linear stability analysis permits one to determine the conditions necessary for the onset of free convection [that is, the critical Rayleigh number (*5*)]. The model of Ray *et al.* differs substantively from earlier free convection models (*6–8*) that assume that the weak convection currents can move either the stones or the soil; this assumption has been shown to be physically unrealistic (*9*). Ray *et al.* assumed that the fluid flows through the soil and stone mixture. Once Rayl[illegible] convection occurs (*10*), it typically form[illegible] hexagonal flow cells in horizontal ground and roll cells or helical coils in sloped terrain. These regular cellular flow patterns can then be impressed on the underlying ice front as shown in Fig. 4, because in areas of downflow, the warmer descending water causes preferential melting. In areas of upflow, the rising cooler water hinders melting of the ice front. Consequently a pattern of regularly spaced peaks and troughs is formed in the underlying ice front that mirrors the polygonal or striped cellular convection patterns in the thawed layer. This pattern is transferred to the ground surface through the process of sorting by well-established mechanisms such as frost push or frost pull (*11*). That is, a freeze-thaw cycle causes the stones to be heaved upward relative to the ice peaks and troughs. This leads to polygonal (predominantly hexagonal) stone patterns for polygo-

K. J. Gleason and W. B. Krantz, Department of Chemical Engineering, University of Colorado, Boulder, CO 80309.
N. Caine, Department of Geography and Institute for Arctic and Alpine Research, University of Colorado, Boulder, CO 80309.
J. H. George, Department of Mathematics, University of Wyoming, Laramie, WY 82071.
R. D. Gunn, Department of Chemical Engineering, University of Wyoming, Laramie, WY 82071.

Table 1. Summary of the comparison between patterned ground field data and the Rayleigh free convection model for nonsubmerged polygons, underwater polygons, and stripes. The model predictions for polygons include both the minimum and maximum pattern width to sorting depth ratio W/D corresponding to flat-to-flat and peak-to-peak determination of W, respectively. The model predictions for stripes include the minimum and maximum pattern width to sorting depth ratio W/D corresponding to negligible and dominant subsurface downslope flow. The number of data points n, mean width to sorting depth ratio $\overline{W/D}$, and standard error S of the mean of W/D (for $n - 1$) method are reported for each pattern type.

Patterned ground	Model predictions (W/D)		Field studies		
	Flat-to-flat or negligible downslope flow	Peak-to-peak or dominant downslope flow	n	$\overline{W/D}$	S
Nonsubmerged polygons	3.1	3.6	23	3.8	0.13
Underwater polygons	4.1	4.8	8	4.8	0.34
Stripes	2.7	3.8	21	3.6	0.27

nal free convection cells, and striped stone patterns for roll or helical coil flow cells. The width of the flow cell at the onset of free convection then determines the width W of the observed stone patterns. The depth of the thawed layer at the onset of free convection L is assumed to correspond to the sorting depth D.

The free convection model of Ray *et al.* explains the initiation, regularity, and characteristic size of some forms of sorted patterned ground. As such, it complements a recently proposed model of Hallet and Prestrud (*12*) for sorting and pattern refinement subsequent to the formation of patterned ground. The model of Ray *et al.* also provides an explanation for the transition from polygons on horizontal ground to stripes on sloped terrain and for the frequency of occurrence of various forms of patterned ground. Since the predicted Rayleigh number for the onset of free convection is smallest for underwater polygons and largest for stripes, the model implies that underwater polygons can occur under less severe conditions, such as lower elevation and smaller soil permeability, than nonsubmerged polygons, whereas stripes will require more severe conditions. These inferences are supported by field observations (*13*). The model also explains the nearly constant ratio of pattern width to sorting depth (W/D) for a particular form of patterned ground (nonsubmerged polygons, underwater polygons, and stripes). The model yields a quantitative prediction of this ratio that can be tested with field measurements if one assumes that the sorting depth of the observed patterns corresponds to the thaw depth at the time when free convection was initiated. For nonsubmerged hexagons, this ratio is predicted to be 3.1 if the width is measured from flat-to-flat and 3.6 if measured from peak-to-peak across a single hexagonal pattern. For underwater hexagons, this ratio is predicted to be 4.1 for the flat-to-flat measurement and 4.8 for the peak-to-peak. Since the sorted stone polygons observed in the field are rarely perfect hexagons, one would expect field measurements of the W/D ratio to fall within the flat-to-flat and peak-to-peak predictions.

In further developing the model for patterned ground, we have focused on the direction of water circulation in the hexagonal cells which ultimately lead to polygonal stone patterns. The fluid circulation can be either up through the center and down the polygonal borders of the cell, or vice versa. Since there is preferential melting in areas of downflow, the first possibility will form an underlying ice front with isolated peaks and continuous hexagonal troughs, whereas the second will lead to isolated troughs with continuous hexagonal ice ridges. Determining the direction of cell circulation provides insight into the sorting process. That is, once the geometry of the underlying ice pattern is inferred from the direction of cell circulation, it is possible to determine whether the stones concentrate over the ice troughs or peaks.

Some investigators (*14–16*) have employed weakly nonlinear stability theory to infer the direction of cell circulation for free convection in a fluid layer (as distinct from a fluid-saturated porous media). These analyses show that asymmetries in the system such as temperature-dependent physical properties can determine the direction of cell circulation. The approach of Palm (*14*) was used to establish the direction of circula-

Fig. 1. Diurnal stone polygon approximately 10 cm wide, near Beartooth Butte in Montana, at an elevation of 3400 m. These small-scale patterns are observed in water-saturated nonsloping ground subject to daily freeze-thaw cycles. Since water exhibits a density maximum at 4°C, unstable density stratification can occur during daily thawing thereby causing polygonal free convection cells. These result in enhanced heat transfer that creates polygonal troughs in the underlying ice. Subsequent nocturnal frost action causes stones to be upthrusted and concentrated over the ice troughs to form a polygonal stone-bordered pattern at the ground surface.

Fig. 2. Diurnal stone stripes approximately 10 cm wide, near Jasper Lake in Montana, at an elevation of 3000 m. These small-scale patterns are observed in water-saturated sloping ground subject to daily freeze-thaw cycles. Unstable density stratification during daily thawing causes roll cells that impress a parallel trough pattern in the underlying ice. Subsequent nocturnal frost action causes stones to be upthrusted and concentrated over the ice troughs to form parallel stone-bordered patterns at the ground surface.

Fig. 3. Underwater polygonal stone patterns, 1.5 m in diameter, at the bottom of a shallow lake, less than 1 m deep, near Medicine Bow Peak in Wyoming, at an elevation of 3300 m. These large-scale patterns are observed in water-saturated soils subject to seasonal freeze-thaw cycles. Unstable density stratification in the thawed soil layer during seasonal thawing causes polygonal cells that impress a polygonal trough pattern in the underlying ice. Subsequent seasonal frost action causes stones to be upthrusted and concentrated over the ice troughs to form a polygonal stone-bordered pattern at the ground surface.

tion for free convection in water-saturated porous media (*17*). Under most conditions, the determining temperature-dependent property for the free convection arising from a thawing frozen soil is the coefficient of volume expansion that passes from its maximum (3.5×10^{-5} per degree Celsius) to minimum (0 per degree Celsius) magnitude in the range 0° to 4°C. In this range, the temperature dependence of this parameter implies cell circulation with upflow in the cell center and downflow along the polygonal borders. The underlying ice front then would appear as isolated ice peaks and continuous polygonal troughs. If stones tend to concentrate over the troughs during sorting, this would lead to stone-bordered polygons, which are the most frequently observed polygonal patterns. Interestingly, if the kinematic viscosity is the dominant temperature-dependent property, the opposite direction of circulation is implied, which would lead to stone pits that indeed are occasionally observed.

In regions where the stones concentrate over ice troughs (Fig. 5), the overall thermal conductivity is higher because rock conducts heat better than soil. Assume that in the freeze following the thaw period that initiated free convection, the sorting process moves some stones over the convection-induced ice troughs. During the next thaw period, conductive heat transfer will be largest where the stone concentration is highest, namely in the regions overlying the initial ice troughs. Thus, heat conduction will re-create ice troughs in the same locations as were defined by free convection during the preceding thaw period (*18*). Subsequent freeze-thaw cycles will cause even more increase in the stone concentration, thereby, with the aid of the consequent enhanced heat conduction, making the evolving patterns ever more prominent until they ultimately become visible on the ground surface.

Two forms of free convection cells can occur in sloped terrain; both result in stone stripes, but are characterized by significantly different pattern width-to-depth ratios. Thawing sloped terrain is subject both to free convection as well as a net subsurface downslope flow. When the latter is negligible, the free convection will be in the form of two-dimensional roll cells whose predicted width-to-depth ratio is 2.7. When the downslope flow is dominant, the free convection will be in the form of helical coils whose predicted width-to-depth ratio is 3.8. A static analog of the latter is a screw whose threads are regularly spaced down its axis. Hence, one would expect field measurements of *W/D* for sorted stone stripes to fall within these two predictions.

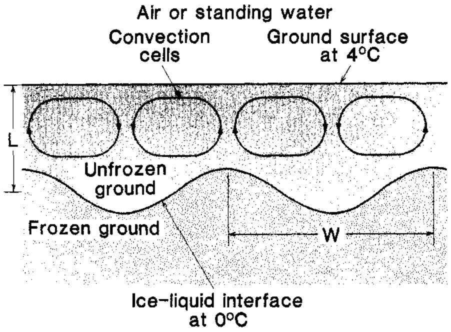

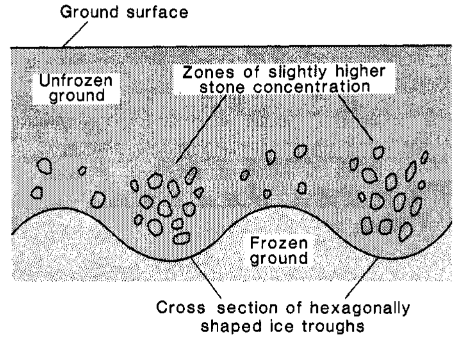

Fig. 4 (left). Schematic showing cross-sectional view of Rayleigh free convection cells in thawed soil layer. Enhanced melting occurs in regions of downflow, thereby impressing a regular trough pattern in the underlying ice. Fig. 5 (right). Schematic showing cross-sectional view of thawed soil layer. Recurrent freeze-thaw cycles cause upthrusting and concentration of stones over the ice troughs formed by Rayleigh free convection thereby eventually creating a stone-bordered pattern at the ground surface.

The ultimate test of any model is how well it agrees with observation. Extensive field data were obtained from the Rocky Mountain region and at selected sites throughout the Northern Hemisphere, including the Arctic Circle. The pattern width W, identified as the distance from the center of one rocky border to the center of the opposite border, was obtained as the average of this measurement in two mutually orthogonal directions. The depth of the active layer at the onset of convection L was assumed to correspond to the sorting depth D. The latter was identified as the distance from the undisturbed ground level to the depth at which no further evidence of sorting was apparent. The data for nonsubmerged polygons and underwater polygons are plotted with W as a function of D (Fig. 6, A and B); Fig. 6A also includes data taken from the literature (*19–21*). The lower and upper lines represent the model predictions reported in terms of flat-to-flat and peak-to-peak widths, respectively. The depth-of-sorting data for the submerged polygons were obtained by trenching sites at a former shallow lake that had been recently drained by the U.S. Forest Service and at a few sites where drainage has occurred naturally. The data for sorted stripes from this investigation and the literature (*21–24*) are plotted in Fig. 6C. In this case, the lower and upper lines correspond to the predictions for negligible and dominant subsurface downslope flow. These results for nonsubmerged polygons, underwater polygons, and stripes are summarized in Table 1. A tabulation of the data used in Fig. 6 is given by Gleason (*17*).

The data are generally supportive of our model, although they exhibit some scatter. An unavoidable source of error is identifying the average thaw depth at the onset of free convection L with the inferred sorting depth D. It is likely that D is less than L, thereby leading to somewhat larger measured W/D ratios. Certainly for striped patterns, some scatter is the result of the unknown magnitude of the subsurface downslope flow. For all three forms of patterned ground considered here, some error is associated with the unknown effects of nonhomogeneous and nonisotropic physical properties which were not taken into account.

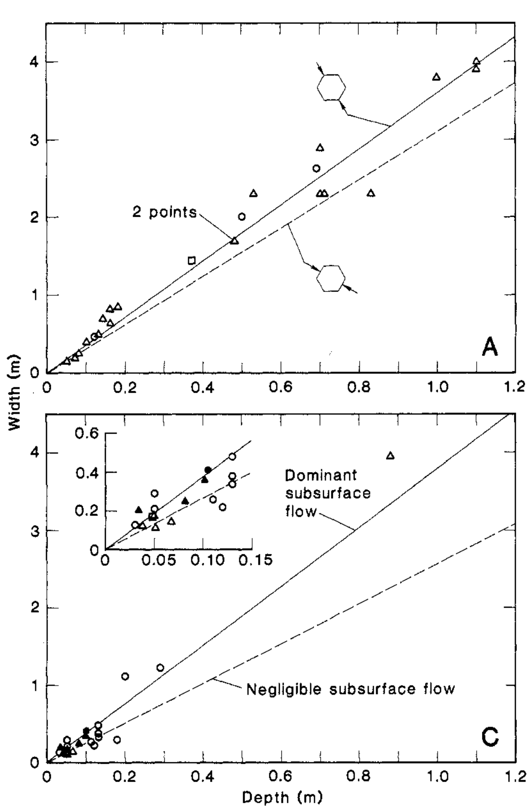

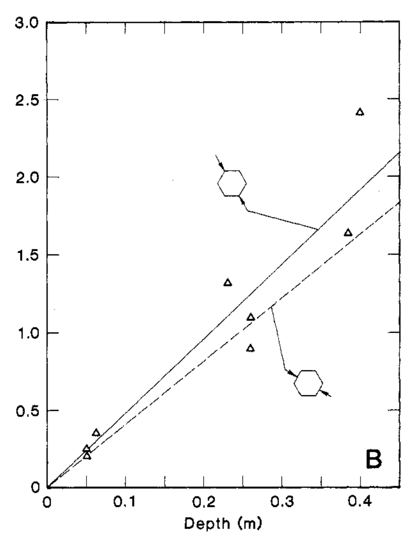

Fig. 6. Comparison between model predictions and field data for the pattern width versus sorting depth for (A) nonsubmerged polygons, (B) underwater polygons, and (C) stripes. The lower and upper lines in (A) and (B) correspond to the Rayleigh free convection model predictions for the minimum and maximum hexagonal pattern width, respectively. The lower and upper lines in (C) correspond to the Rayleigh free convection model predictions for negligible and dominant subsurface downslope flow, respectively. Symbols in (A) represent this report (△), Schunke (○) (*19, 20*), and Stingl (□) (*21*); in (B), this report; and in (C), this report (△), Hall (○) (*22*), Lundqvist (□) (*23*), Warburton (▲) (*24*), and Stingl (●) (*21*).

REFERENCES AND NOTES

1. R. J. Ray, W. B. Krantz, T. N. Caine, R. D. Gunn, *J. Glaciol.* **29**, 317 (1983).
2. ———, in *Permafrost: Proceedings of the Fourth International Conference* (National Academy of Sciences, Washington, DC, 1983), pp. 1036–1041.
3. Rayleigh free convection refers to fluid flow generated by unstable density stratification.
4. Free convection may also be possible during upfreezing; however, we do not consider this to be essential to the model for the origin and regularity of patterned ground.
5. The dimensionless Rayleigh number is a measure of the ratio of the buoyancy force driving free convection to a measure of the viscous and heat conduction mechanisms that inhibit free convection. The critical Rayleigh number then defines the parametric conditions necessary for the onset of free convection.
6. O. Nordenskjöld, *Die Polarwelt und ihre Nachbarländer* (Teubner, Leipzig, 1909), pp. 63–64.
7. A. R. Low, *Nature (London)* **115**, 299 (1925).
8. E. Palm and M. Tveitereid, *Nor. Geogr. Tidsskr.* **31**, 145 (1977).
9. C. S. Elton, *J. Geol. Soc. London* **83**, 163 (1927).
10. Sites that ultimately display patterned ground are assumed to arrive at the critical Rayleigh number condition by the action of numerous freeze-thaw cycles that increase the soil permeability and perhaps change other key parameters appearing in the Rayleigh number so that free convection eventually becomes possible; for this reason, the pattern width-to-depth ratio is seen to correspond to that defined by the particular wave number associated with the critical Rayleigh number.
11. Frost push is the upward movement of stones because of the formation of segregation ice beneath them. Frost pull is the upward movement of stones associated with heaving of a frozen soil layer to which the stone is frozen [L. W. Price, *Assoc. Am. Geogr. Comm. Coll. Geogr. Resour. Pap. 14* (1972), p. 27].
12. B. Hallet and S. Prestrud, *Quat. Res.*, in press.
13. The authors have observed many sites where underwater polygons exist in the absence of nonsubmerged polygons. At a few sites in the Rocky Mountains, nonsubmerged polygons were observed along with underwater polygons, but at approximately 300 m higher elevation. Sites displaying

large-scale stripes are observed relatively infrequently.
14. E. Palm, *J. Fluid Mech.* **8**, 183 (1960).
15. L. A. Segel, *ibid.* **21**, 359 (1965).
16. R. Krishnamurti, *ibid.* **33**, 445 (1968).
17. K. J. Gleason, thesis, University of Colorado, Boulder (1984). (In table 6.1, the depth of the datum for Macquarie Island in Australia should be 0.08 m, not 0.80 m.)
18. It is for this reason that the particular wave number associated with the critical Rayleigh number defines the pattern width-to-depth ratio even though conditions prevailing subsequent to the onset of free convection may permit Rayleigh numbers, and thereby wave numbers, above those defined by critical conditions.
19. E. Schunke, *Abh. Akad. Wiss. Göttingen Math. Phys. Kl. (Folge 3)* **30**, 1 (1975).
20. ——, *Ges. Erdkd. Berlin Z.* **106**, 47 (1975).
21. H. Stingl, *Abh. Akad. Wiss. Göttingen Math. Phys. Kl. (Folge 3)* **29**, 249 (1974).
22. K. Hall, *Earth Surf. Processes Landforms* **8**, 115 (1983).
23. J. Lundqvist, *Sver. Geol. Unders. Ser. C* **55**, 4 (1962).
24. J. Warburton, thesis, University of Colorado, Boulder (1985).
25. Supported in part by NSF grant DPP-8210156, the Council for Research and Creative Work of the University of Colorado, a University of Colorado Graduate School Fellowship, and Graduate School Foundation Fund Award to K.J.G., the University of Notre Dame Keating-Crawford Chair Award to W.B.K., and Army contract DAAG 29-84-K-0002 to J.H.G.

30 July 1985; accepted 6 January 1986

Anti-Idiotypic Antibody Vaccine for Type B Viral Hepatitis in Chimpanzees

RONALD C. KENNEDY, JORG W. EICHBERG, ROBERT E. LANFORD, GORDON R. DREESMAN

Anti-idiotypic antibodies (anti-Id) that contain an internal image component that mimics the surface antigen of hepatitis B virus (HBsAg) were used to immunize chimpanzees. Four injections of the rabbit anti-Id preparation elicited an antibody response to HBsAg (anti-HBs). The antibody specificity appeared to be against the anti-Id, since the anti-Id immunogen was shown to bind the chimpanzee anti-HBs. Two chimpanzees immunized with the anti-Id, along with two control animals that were either untreated or received a nonimmune rabbit immunoglobulin G preparation, were challenged with infectious hepatitis B virus. Both control chimpanzees developed clinical and serological characteristics consistent with an active hepatitis B virus infection, whereas the two anti-Id treated chimpanzees were protected from infection. Since chimpanzees provide a relevant model of a human response to hepatitis B virus immunization and infection, these results indicate that anti-Id preparations such as that described here might be candidates for vaccines against human diseases.

A SUBUNIT VACCINE FOR HEPATITIS B virus (HBV) is now available and is produced by purifying HBV surface antigen (HBsAg) from the plasma of persons chronically infected with HBV. Although this vaccine is safe and effective, its high cost is likely to preclude its use in developing countries where HBV and its sequelae constitute a major health problem. Several alternative approaches to the preparation of HBsAg vaccines are under investigation. In one, DNA fragments of HBV are cloned into suitable vectors (*1, 2*). Studies in chimpanzees have demonstrated that this recombinant HBsAg approach is a possible means for a vaccine production (*3–5*). In another approach, synthetic peptides that contain amino acid sequences analogous to those associated with the major protein component of HBsAg are used (*6*). However, these synthetic HBsAg peptides may only partially protect chimpanzees from challenge with infectious HBV (*7*). In a third approach, being studied at our laboratories, an anti-idiotypic antibody (anti-Id) preparation that represents the internal image of HBsAg is used as the vaccine.

An idiotype or idiotypic determinant (Id) defines the variable (V) region of an antibody molecule. Initial studies by Kunkel *et al.* (*8*) and Oudin and Michael (*9*) characterized these antigenic determinants on human and rabbit antibodies, respectively, by generating anti-Id reagents. Id, along with homologous anti-Id, are thought to be components of a network of complex reactions that regulates a given immune response. Initially proposed by Jerne (*10*), Id networks have been implicated in regulating the immune response to a wide variety of haptens and protein or carbohydrate antigens (*11, 12*). More recently, anti-Id have been used to induce an immune response to antigens associated with a large number of pathogens (*13*). Previous studies at our laboratories (*14*) led to the characterization of a common Id on human antibodies to HBsAg. The anti-Id produced in rabbits against the human Id antibody to HBsAg appeared to contain an internal image component that mimicked HBsAg: This was deduced from (i) the detection of an interspecies Id cross-reaction associated with antibodies to HBsAg (*15*); and (ii) the production in mice of antibodies to HBsAg that serologically resembled the human Id antibody to HBsAg produced by injecting anti-Id alone (*16, 17*). Together these data indicated that this internal image anti-Id might be useful as a vaccine against HBV.

In the present studies, human antibodies to HBsAg served as the idiotype or first antibody (Ab-1) that was injected into rabbits to produce the anti-Id or second antibody (Ab-2). The rabbit anti-Id or Ab-2 was tested for its vaccine potential. Two chimpanzees that received four injections of affinity-purified rabbit anti-Id developed a detectable anti-HBs response 1 week (week 12) after the final immunization (Fig. 1). Although 1 mg of anti-Id per injection represents a large dose when compared to conventional vaccines, it is noteworthy that the anti-Id is a polyclonal antibody preparation and only a percentage of the total anti-Id may represent the internal image. Presumably an internal image anti-Id that was produced monoclonally might contain a larger proportion of internal image anti-Id so that a lower dose of vaccine could be used for vaccination. One chimpanzee (X-33) that was injected with nonimmune rabbit immunoglobulin G (IgG) on a similar schedule did not develop an anti-HBs response before being challenged with infectious HBV. In addition, an untreated control chimpanzee (X-188), seronegative for anti-HBs, was included in this study and showed no antibody response to HBV infection. These data suggested that the anti-Id immunization was responsible for inducing anti-HBs.

To ascertain whether the chimpanzee anti–HBs was associated with an anti-Id response to the rabbit anti-Id (a chimpanzee anti–anti-Id response), serum containing anti-HBs was obtained from each chimpanzee before it was challenged with virus (week 13 to 23). This serum was pooled and repeatedly adsorbed over an immunoadsorbent column coated with nonimmune rabbit IgG. The presence of anti-isotypic and anti-allotypic activity along with anti-idiotypic activity against the rabbit anti-Id was determined by a direct binding radioimmunoassay (RIA). An isotype is an antigen that determines the class and subclass differences found on immunoglobulin molecules within

Department of Virology and Immunology, Southwest Foundation for Biomedical Research, San Antonio, TX 78284.